Electronic Supplementary Material (ESI) for Journal of Materials Chemistry C.

Supplementary information

Hydro-tunable CZTO/SWCNT/PVA/PDMS hybrid composites for smart green EMI shielding

Prem Pal Singh, Anurima De, Bhanu Bhusan Khatua*

Materials Science Centre, Indian Institute of Technology Kharagpur, Kharagpur-721302, India.

***Corresponding author**

Prof. B. B. Khatua (Email: khatuabb@matsc.iitkgp.ac.in)

Materials Science Centre, Indian Institute of Technology, Kharagpur – 721302, India

Tel.: +91- 3222-283982

Supplementary discussion

1. Key challenges and future perspective

a. Since most of the water was absorbed by the surface and near-surface PVA particles whereas hydrophobic PDMS layers were protected deep inside PVA particles. As a result, we needed a polymer composite configuration that allows water to penetrate throughout bulk in order to achieve maximum water loading for a wider tuning window of EMI SE.

b. Controlling the water retention ability (shelf life) of PVA particles is also a very difficult task because open-air applications cause continuous water evaporation.

1. **XRD of CZTO and VSM of SWCNTs, OM of PVA particles and particle size distribution of CZTO**

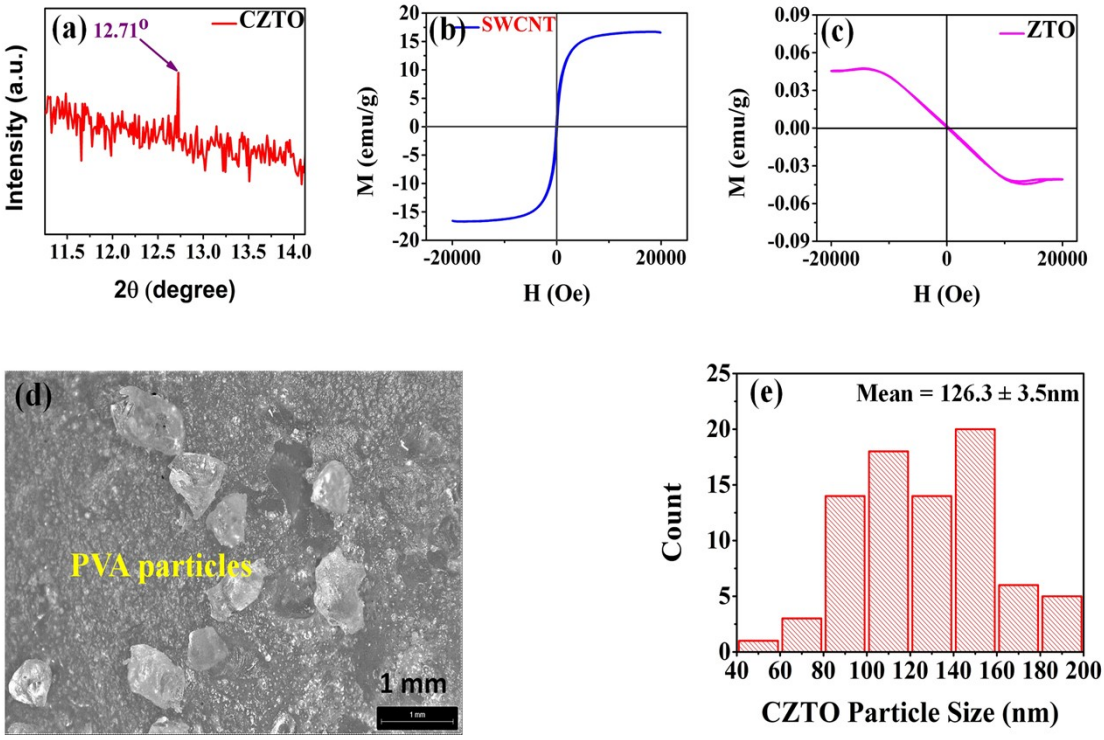

Fig. 1. (a) XRD spectrum of CZTO showing peak for carbon, (b, c) M-H curve of SWCNT and ZTO, respectively, (d) Stereo-optical microscope image of used PVA particles, (e) histogram of CZTO particle size distribution

2. Elemental characterization of CZTO, SWCNT and composite

2.1. EDS results

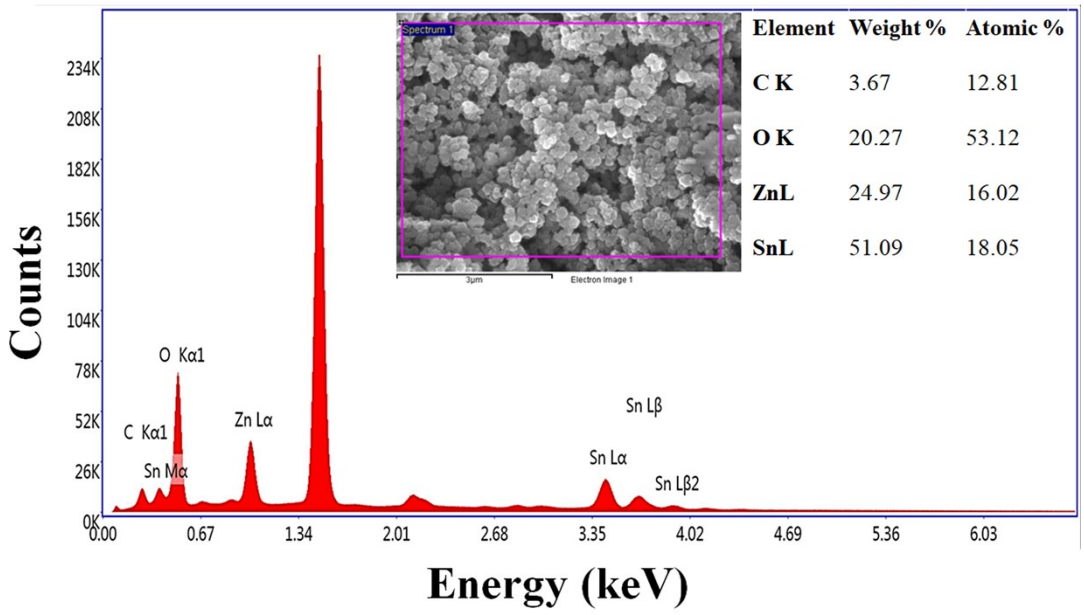

Fig. 2. EDS elemental distribution spectrum of CZTO

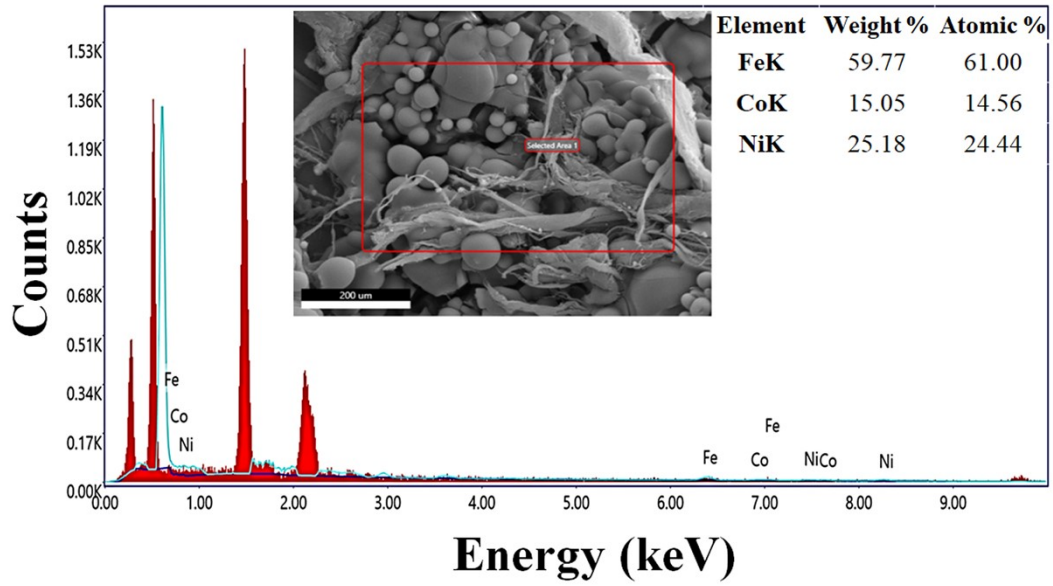

Fig. 3. EDS elemental distribution spectrum of SWCNT

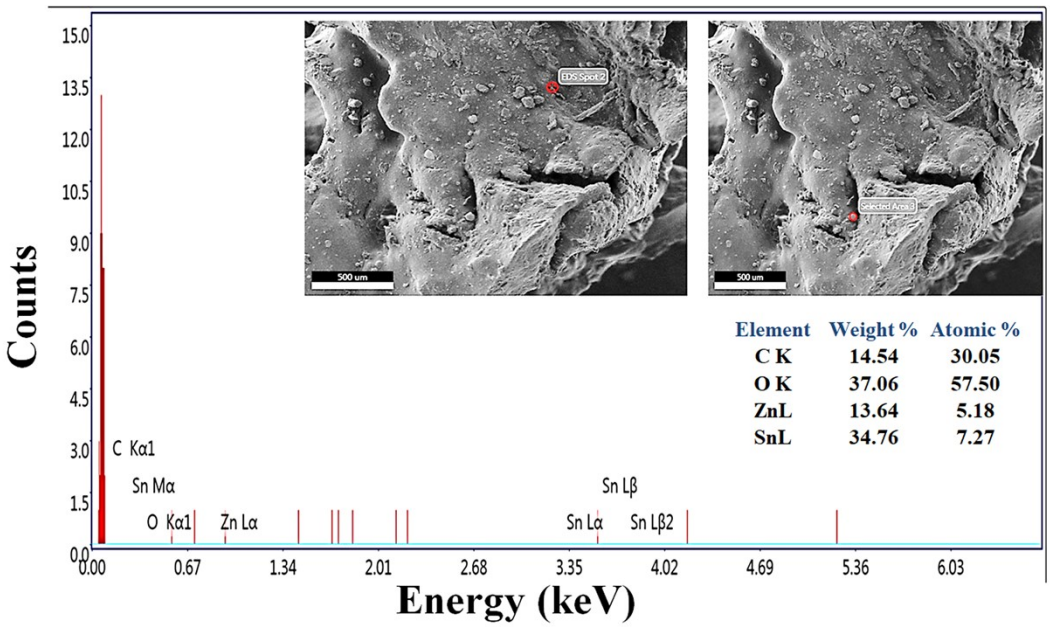

Fig. 4. EDS analysis of CZTO distribution on the cryo-fractured composite sample

3. Electromagnetic Shielding

The following equations theoretically provide the reflection, absorption, and multiple reflection shielding components of the total electromagnetic shielding efficiency [1-3]:

* Reflection shielding

$$SE_R(dB) = 10 \times \log_{10}\left(\frac{\sigma_{DC}}{16\omega\varepsilon_o\mu^*}\right) \quad (1S)$$

* Absorption shielding

$$SE_A\ (dB) = 20\left(\frac{t}{\delta}\right)\log e = 8.68\frac{t}{\delta} = 8.68t\left(\frac{\sigma_{DC}\mu^*\omega}{2}\right)^{1/2} \quad (2S)$$

* Multiple or secondary reflection shielding

$$SE_M = 20\log\left|\left(1-10^{(SE_A/10)}\right)\right| = 20\log\left(1-e^{-2d/\delta}\right) \quad (3S)$$

Where, σ_{DC} is the DC conductivity (S/cm), ε_o is the permittivity vacuum, $\omega (= 2\pi f)$ is the angular and f is the frequency, t is the composite thickness, δ is the skin depth and μ^* is the complex permeability.

$$R = |S_{11}|^2 = |S_{22}|^2 \tag{4S}$$

$$T = |S_{21}|^2 = |S_{12}|^2 \tag{5S}$$

$$A + R + T = 1 \tag{6S}$$

$$SE_R = -10\log_{10}(1-R) = -10\log_{10}\left(1-|S_{11}|^2\right) \tag{7S}$$

$$SE_A = -10\log_{10}\left(\frac{T}{1-R}\right) = -10\log_{10}\left(\frac{|S_{12}|^2}{1-|S_{11}|^2}\right) \tag{8S}$$

The total EMI SE ($EMI\ SE_T$) mathematically, can be expressed as:

$$EMI\ SE_T = SE_A + SE_R = -10\log_{10}(T) = -10\log_{10}|S_{21}|^2 \tag{9S}$$

Green index [4]:

$$g_s = \frac{1}{R} - \frac{T}{R} - 1 \tag{10S}$$

Reflection loss

$$RL(dB) = 20 \times \log_{10}\frac{|Z_{in} - Z_o|}{|Z_{in} + Z_o|} \tag{11S}$$

Where Z_{in} is the normalized input impedance of shield and Z_o is the impedance of free space. The Z_{in} can be expressed as

$$Z_{in} = \sqrt{\frac{\mu_r^*}{\varepsilon_r^*}} Tanh\left[j\frac{2\pi}{c}\sqrt{\mu_r^*\varepsilon_r^*}\, fd \right] \tag{12S}$$

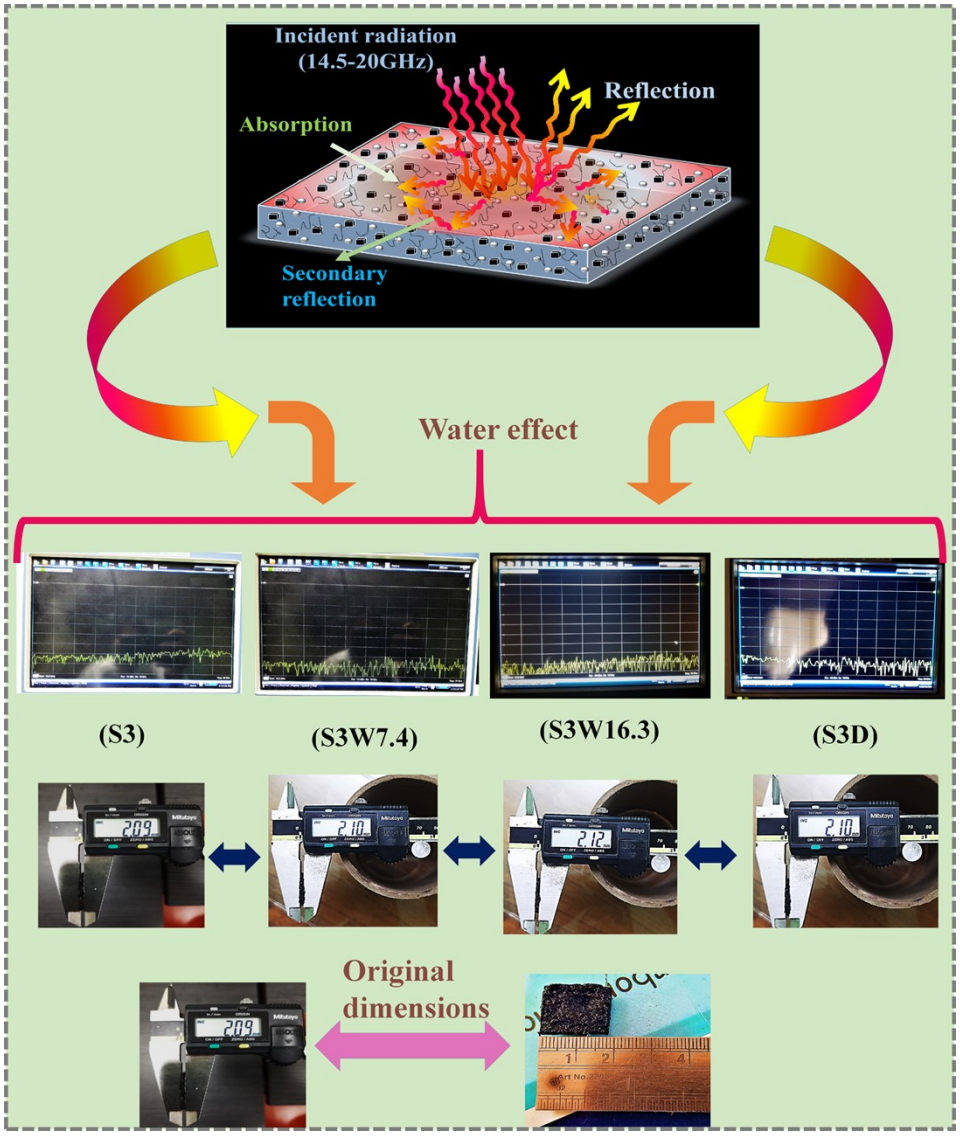

Fig. 5. Real time data collection on VNA, demonstrating hydro effect of EMI shielding performance

3.1. Effect of SWCNT loading on shielding performance

Table 1. SWCNT/CZTO/PDMS composites with increasing SWCNT content

Composite name	Description
C1	3wt.% SWCNT/5wt.% CZTO/PDMS
C2	5wt.% SWCNT/5wt.% CZTO/PDMS
C3	7wt.% SWCNT/5wt.% CZTO/PDMS

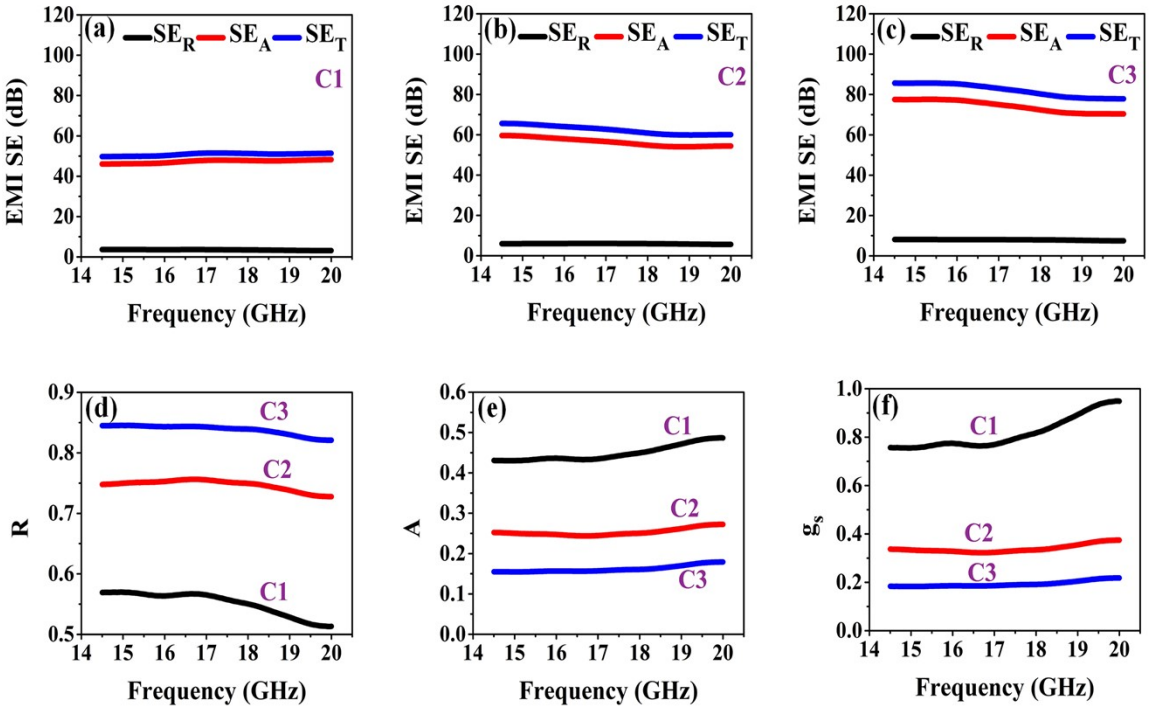

Fig. 6. (a-c) EMI SE variation against frequency on increasing SWCNT in C1, C2 and C3 composites, (d-f) reflection coefficient, absorption coefficient and green shielding index versus frequency of C1, C2 and C3 composites

3.2. EMI shielding of individual components in PDMS

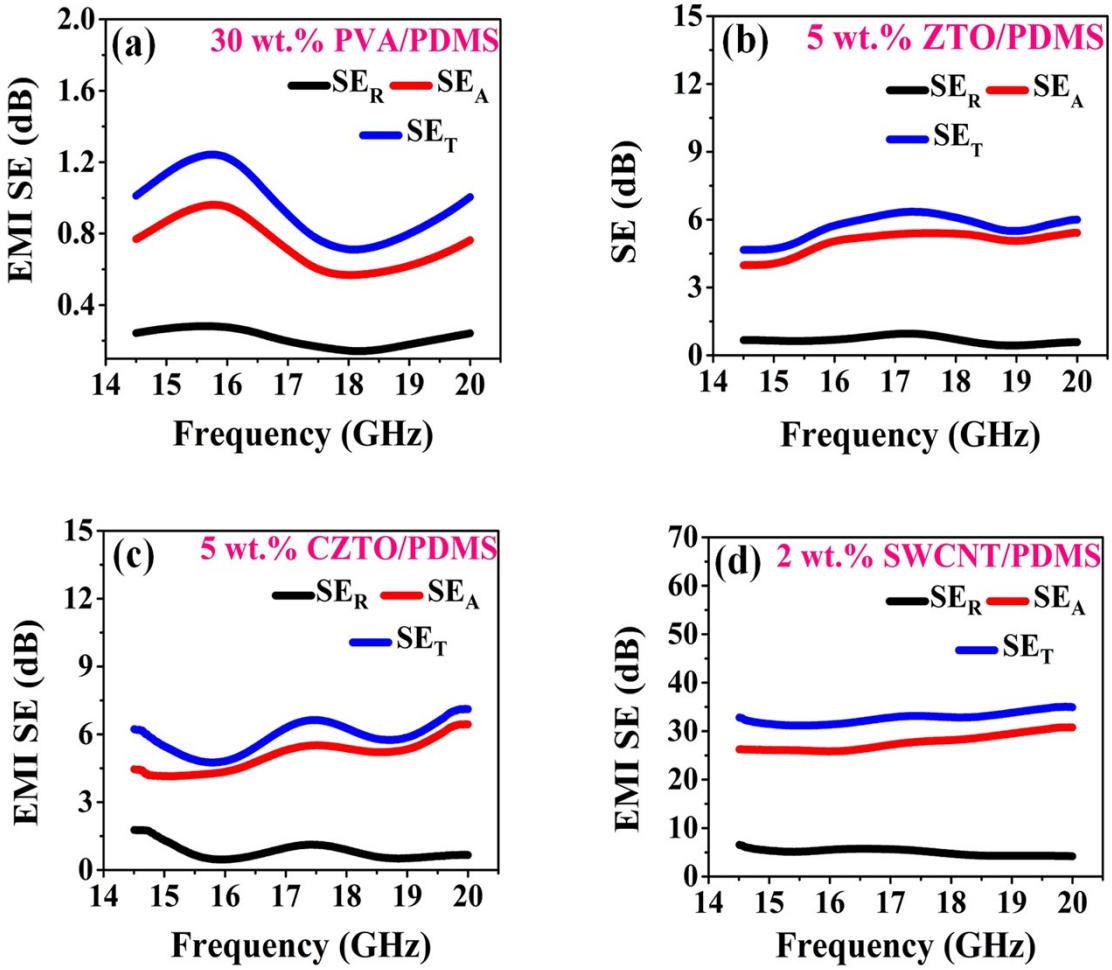

Fig. 7. Total, absorption and reflection shielding versus frequency for (a) PVA/PDMS, (b) ZTO/PDMS, (c) CZTO/PDMS and (d) SWCNT/PDMS composites.

3.3. Electromagnetic response of individual component composites

a. Complex permittivity

$$\varepsilon^* = \varepsilon' + i\varepsilon'' \tag{13S}$$

Magnitude:

$$\varepsilon^* = \sqrt{(\varepsilon')^2 + (\varepsilon'')^2} \tag{14S}$$

b. Complex permeability

$$\mu^* = \mu' + i\mu'' \tag{15S}$$

Magnitude:

$$\mu^* = \sqrt{(\mu')^2 + (\mu'')^2} \tag{16S}$$

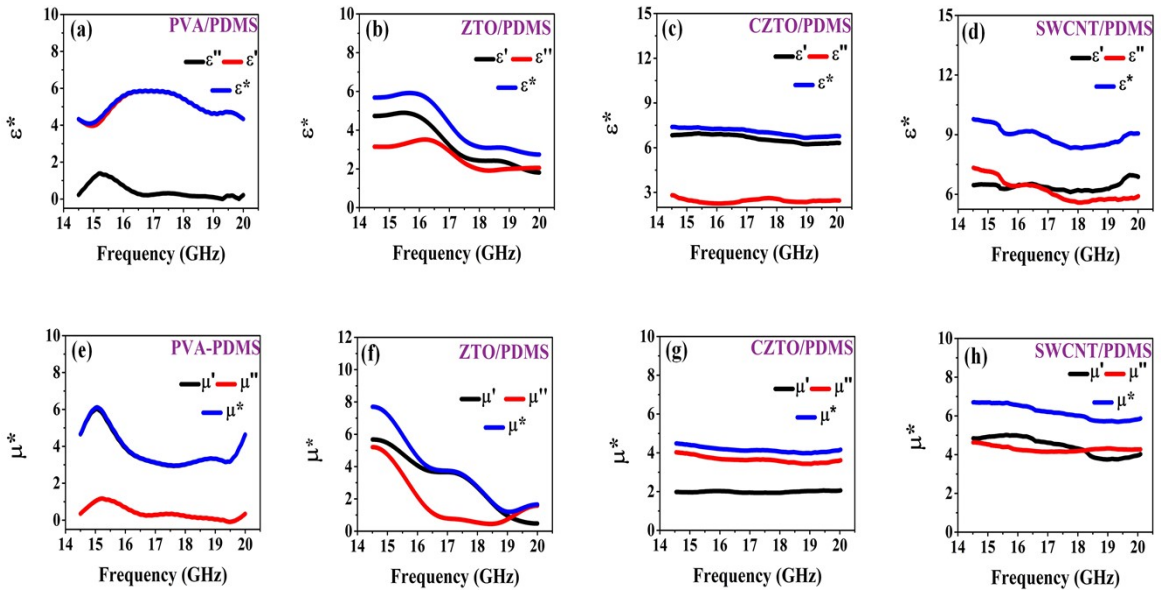

Fig. 8. (a – d) complex permittivity vs. frequency; (e– h) complex permeability vs. frequency of PVA/PDMS, ZTO/PDMS, CZTO/PDMS, SWCNT/PDMS, respectively.

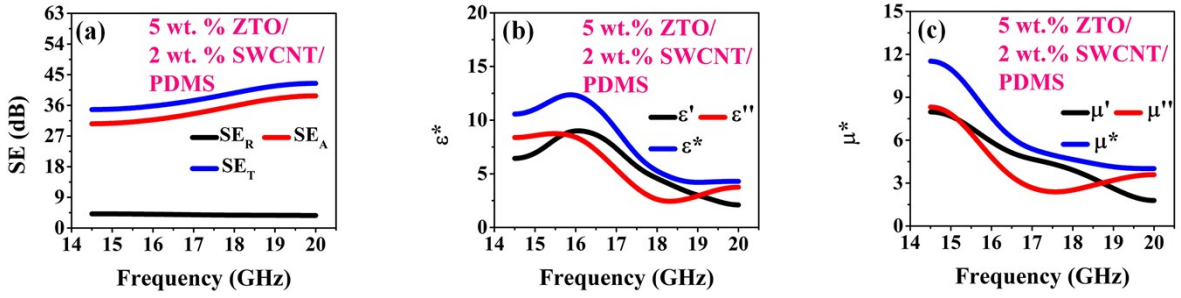

Fig. 9. (a) SE performance, (b) complex dielectric permittivity and (c) complex magnetic permeability of ZTO(5wt.%)/SWCNT(2wt%)/PDMS composite.

Effect excluded volume and moisture loss tangents, AC conductivity and attenuation constant

The dissipation factors i.e. dielectric loss tangent $(Tan\delta_{\varepsilon} = \varepsilon^{''}/\varepsilon^{'})$ and magnetic loss tangent $(Tan\delta_{\mu} = \mu^{''}/\mu^{'})$ represents the electrical and magnetic energy losses. The dielectric loss tangent represents the electrical energy loss by means of different processes such as electrical conduction, dielectric polarization relaxation, dielectric resonance, etc.[1]. Whereas magnetic loss tangent represents magnetic energy loss by means of eddy current, domain wall resonances (domain wall resonance and electron spin resonance), and hysteresis losses, etc.[1, 2]. The loss tangent results are plotted in fig. 10a, c for S1, S2, and S3 samples, as depicted both dielectric and magnetic loss tangents increased with PVA loading and non-uniformly vary with frequency in the 14.5 to 20 GHz range. Moreover, AC conductivity $(\sigma_{AC} = 2\pi f\varepsilon_o\varepsilon^{''})$ measures the total electrical conduction loss under influence of the high-frequency electromagnetic field. Fig. 10b displays the AC conductivity of S 1, S2, and S3 composite samples, which increased about 3 times at 20 GHz for the S3 than S1 on increasing 30 wt.% PVA incorporation.

Although, in one shot, the overall dielectric and magnetic loss of composite is determined by the attenuation constant, which was calculated for composite samples by following the equation (17S)[1]:

$$\alpha = \frac{\sqrt{2}\pi f}{c} \times \sqrt{(\varepsilon^{''}\mu^{''} - \varepsilon^{'}\mu^{'}) + \sqrt{(\varepsilon^{''}\mu^{''} - \varepsilon^{'}\mu^{'})^2 + (\varepsilon^{''}\mu^{''} + \varepsilon^{'}\mu^{'})^2}} \quad (17S)$$

Where f is the frequency and c is the light velocity. Fig. 10d depicts the attenuation behavior for S1, S2 and S3 composites. The attenuation constant for samples S1 (2565.64) and S2 (5289.01) and S3 (7619.8) at 20 GHz is increased with PVA loading as well as with frequency validating

the same trend (increasing) of EMI shielding effectiveness for S1, S2, and S3 composites. Similarly, these parameters were measured to investigate the changing of electromagnetic nature of composite S3 on allowing different content of water absorption. The obtained results were plotted in fig. 11, which depicted the absorbed water content and frequency-dependent variations. Fig. 11a and 11c, depict the increase of both dielectric and magnetic loss tangents on increasing the water loading and partially recovering to its initial state after drying. Similarly, the AC conductivity and attenuation constant attains the same trends on increasing water loading and recovering on drying (Fig. 11 b, d).

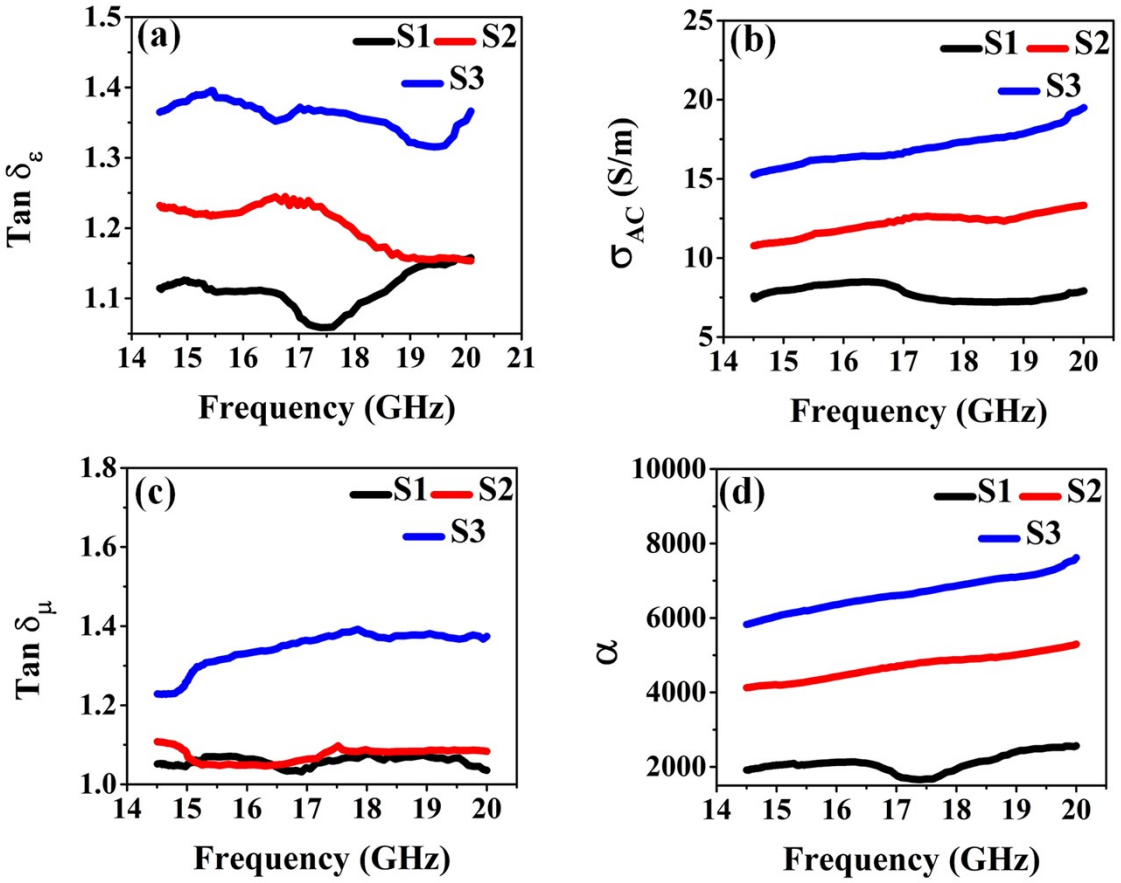

Fig. 10. (a), (c) dielectric loss tangents vs. frequency for all samples, (b, d) AC conductivity and attenuation constant vs frequency for all samples.

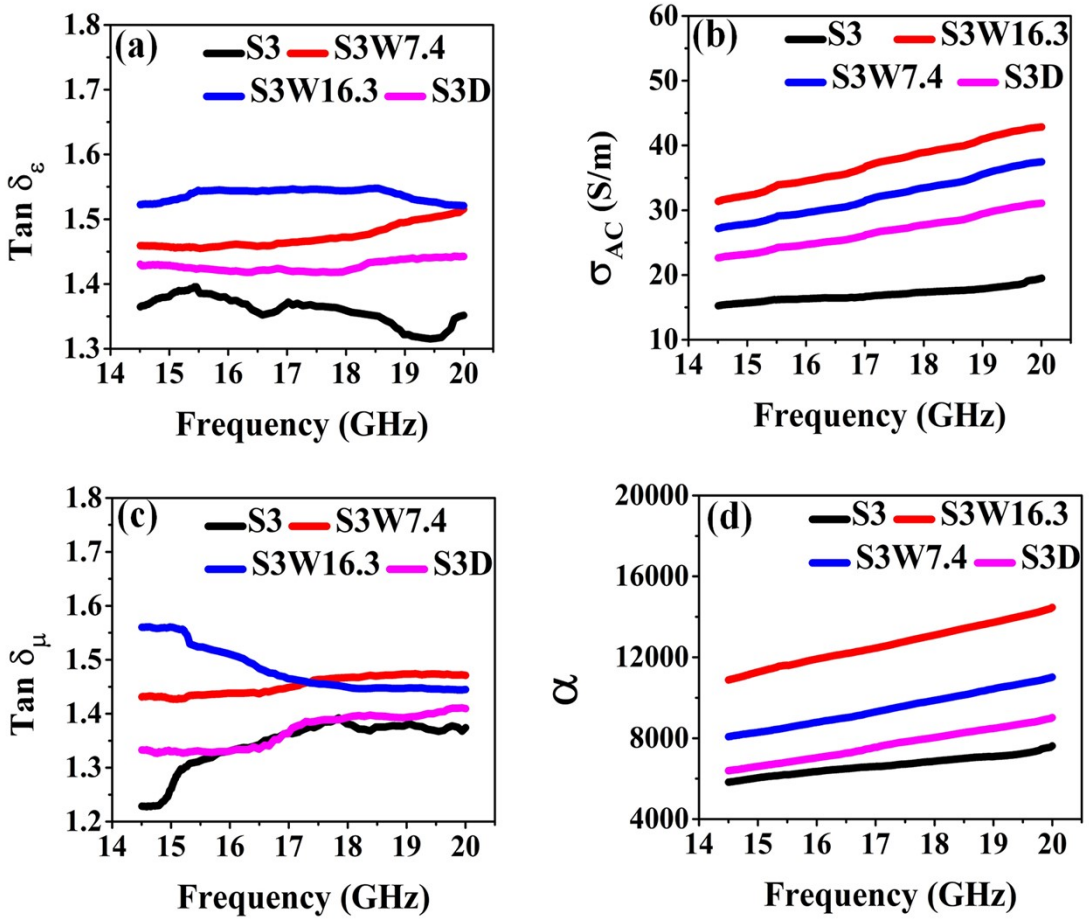

Fig. 11. (a, c) Dielectric loss and magnetic loss, (b, d) conduction loss (AC conductivity) and total loss (attenuation constant) in extended Ku frequency (14.5 – 20 GHz) band at different water content loading, respectively.

4. More on reflection and absorption shielding explanation

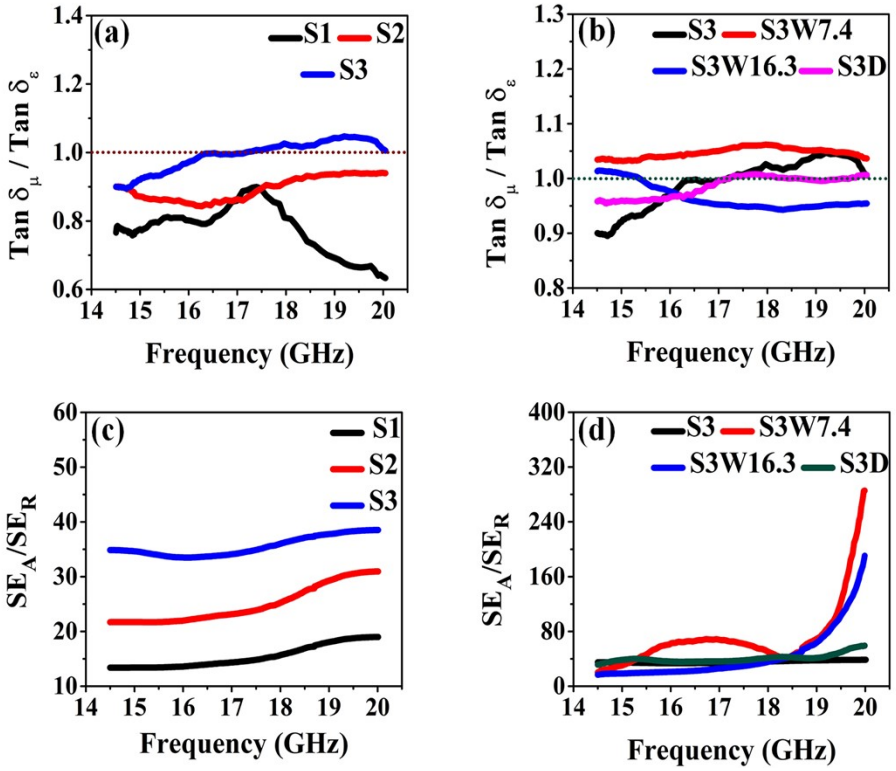

Fig. 12. (a) Excluded volume tunable impedance matching (magnetic loss tangent to dielectric loss tangent ratio) of S1, S2, and S3 composite versus frequency, (b) Hydro content tunable impedance matching for S3, S3W7.4, S3W16.3, and S3D composites versus frequency.

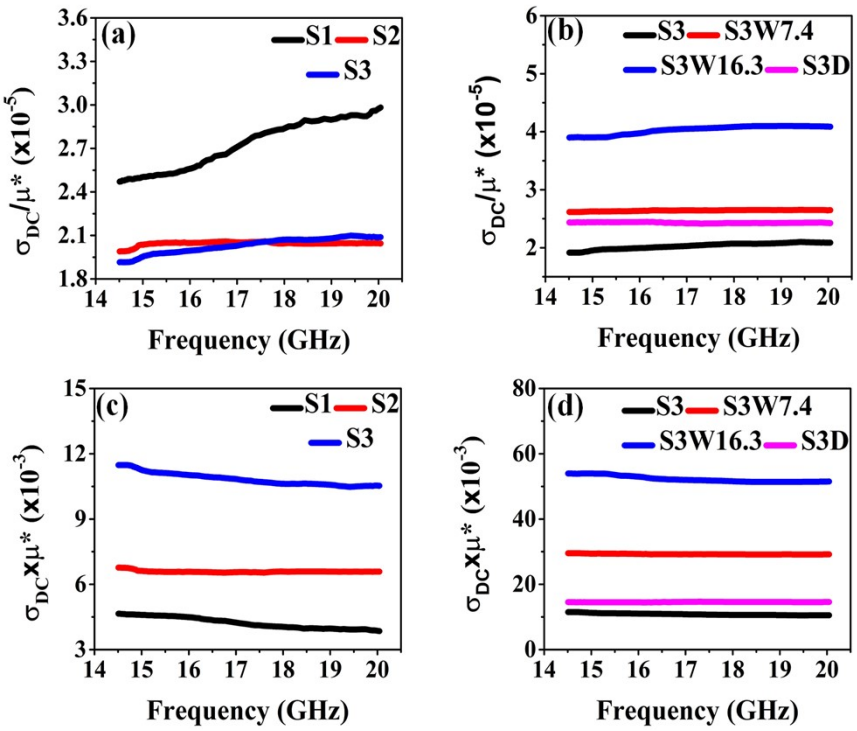

Fig. 13. (a, b) DC conductivity to complex permeability ratio, (c, d) DC conductivity to complex permeability product versus frequency, respectively, for all samples.

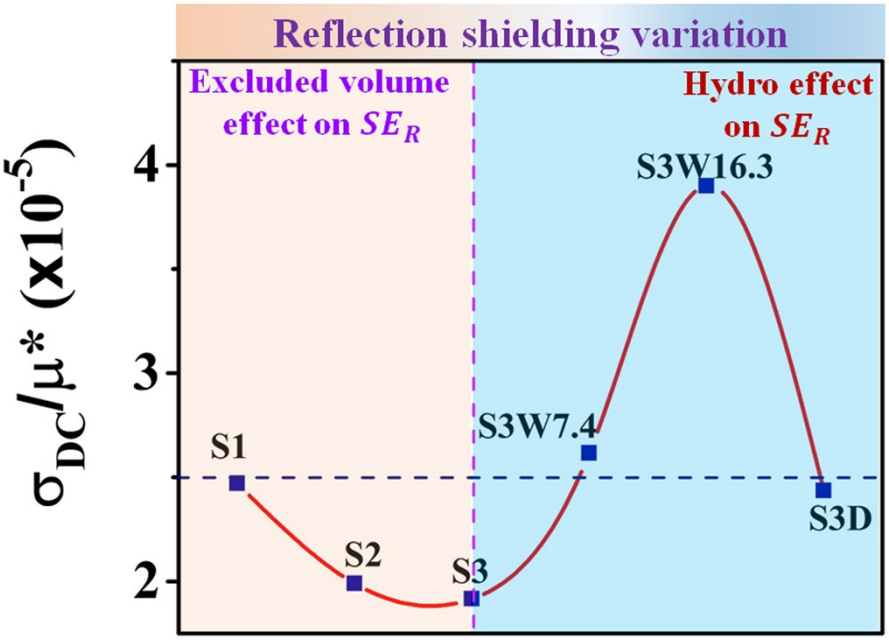

Fig. 14. Reflection shielding variation with DC conductivity to complex permeability ratio at 14.5 GHz frequency.

Table 2 Comparison of typical EMI shielding performance of recently published research articles

Composite systems	Type - Thickness	Type of EMI Tunability	Stimulus	Green Shielding	Max. SE (dB)	Ref. in manu script
CZTO/SWCNT/PVA/PDMS -1	Bulk - 2.1 mm	Intrinsic	Excluded volume	Yes	74.81	This work
CZTO/SWCNT/PVA/PDMS -2	Bulk - 2.1 mm	Extrinsic	Hydro	Yes	92.4	This work
HTPB-BA and HTPB-BA-CNT	Film- 2 mm	Extrinsic	Mechanical stress/ Temperature	Not mentioned	47.28	[1]
PDMS/FRS	Foam - 10 mm	Extrinsic	Mechanical stress	Not mentioned	35.83	[2]
SnS/SnO2@C	Bulk – 5 mm	Extrinsic	Voltage	Not mentioned	Not mentioned	[3]
PIF/CNT	Foam - 15 mm	Extrinsic	Hydro	Not mentioned	69.3	[4]
G-RGO/NT/NW-G-2	sandwich-2.2 mm	Extrinsic	Hydro	Not mentioned	38	[32]
CNT/CNF	Foam - 5 mm	Extrinsic	Mechanical stress	Not mentioned	30	[33]
PU@Cu fabrics	Fabric - 39 μm	Extrinsic	Mechanical stress	Not mentioned	63.5	[34]
wood-derived lamellar carbon aerogel	Foam	Extrinsic	Mechanical stress	Not mentioned	29	[35]
Magnetic metal–CNT arrays	Fabric	Extrinsic	Voltage	Not mentioned	68.1	[36]
TPI-M/CF	Foam-10mm	Extrinsic	Mechanical stress	Not mentioned	44.7	[37]

5. References

1. M. Wang, X.H. Tang, J.H. Cai, H. Wu, J.B. Shen, S.Y. Guo, Carbon, 2021, **177**, 377-402.

2. W.L. Song, M.S. Cao, M.M. Lu, S. Bi, C.Y. Wang, J. Liu, J. Yuan, L.Z. Fan, Carbon, 2014, **1**, 67-76.

3. S. Kim, Y.S. Jang, T. Oh, S.K. Lee, D.Y. Yoo, J. of Mat. Res. and Tech. 2022, https://doi.org/10.1016/j.jmrt.2022.07.041Get

4. X.X. Wang, J.C. Shu, W.Q. Cao, M. Zhang, J. Yuan, M.S. Cao, Chem. Engi. J, 2019, 1, 369:1068-77.